Acid mine drainage sources and hydrogeochemistry at the Yatani mine, Yamagata, Japan: A geochemical and isotopic study

Shingo Tomiyama[a,b,*], Toshihumi Igarashi[a], Carlito Baltazar Tabelin[a], Pawit Tangviroon[a], Hiroyuki Ii[c]

a Division of Sustainable Resources Engineering, Faculty of Engineering, Hokkaido University, Sapporo, Japan 060-8628

b Mitsubishi Materials Corporation, 3-2, Otemachi 1-chome, Chiyoda-ku, Tokyo, Japan 100-8117

c Graduate School of Systems Engineering, Wakayama University, 930 Sakaedani, Wakayama, Japan 640-8510

*Corresponding author e-mail: tomiyama@mmc.co.jp, TEL +81-11-706-8191

1. Introduction

There are more than 5,500 closed or abandoned non-ferrous metal mines in Japan, many of which produce acid mine drainage (AMD; Ueda and Masuda, 2005; Herrera et al., 2007a, b). AMD is not only acidic but may also contain toxic contaminants such as Cu, Pb, Zn, and As, and is a serious environmental problem in many active, closed, and abandoned mines (Younger, 2001; Gault et al., 2005; Molson et al., 2005; Boulabah et al., 2006; Lim et al., 2008; Hien et al., 2012; Hierro et al., 2014; Skierszkan et al., 2016; Zhao et al., 2017).

AMD typically forms in old mine workings (mining levels, drifts and shafts), waste-rock dumps, and tailings storage facilities where sulfide minerals such as pyrite are exposed to oxidizing conditions (Singer and Stumm, 1970; Lowson, 1982; Tabelin et al., 2017a, b). The problem is commonly managed by neutralization (Kalin et al., 2006), precipitating heavy metals with basic materials such as limestone, lime, or caustic soda.

29 This method has been effectively used in many closed or abandoned mine sites over the
30 last 40 years, at a total subsidiary aid cost of ~70 billion JPY (~770 million USD)
31 (Kawabe, 2017). Water treatment is not a sustainable solution owing to its continuing
32 high cost. Land surface remediation and wetland treatment have been implemented in
33 Japan (Tomiyama et al., 2016a; Ogino, 2017; Okimoto et al., 2017), but again the cost
34 is unsustainable. Now, a "green remediation of abandoned mines" program is to be
35 implemented with the goal of returning mine landscapes to their pre-mining state, while
36 also reducing treatment costs with a variety of techniques including the sealing of
37 mining levels and wetland treatment (Nagai, 2018). An understanding of the origin and
38 flow of groundwater in abandoned mines is essential for the development of
39 countermeasures such as back-filling and sealing of surfaces in recharge areas.
40 Groundwater flow modeling, based on the monitoring of changes in geochemistry of
41 water percolating into mines, has provided useful information in the development of an
42 AMD mitigation strategy (Tomiyama et al., 2010a). Previous studies have characterized
43 geochemical and isotopic compositions of AMD in Japan (Iwatsuki and Yoshida, 1999;
44 Okumura, 2003; Mahara et al., 2006; Tomiyama et al., 2010b; Yamaguchi et al., 2015;
45 Tomiyama et al., 2016b) and other countries (Wunsch et al., 1999; Hazen et al., 2002;
46 Sracek et al., 2004; Casiot et al., 2005; Lim et al., 2008; Gammons et al., 2010; Pabst et
47 al., 2018; Ramasamy et al., 2018). Further information could be provided by studies of
48 the origin and hydrogeochemistry of AMD in mining areas where water samples can be
49 collected from inside mining levels and surface sites.
50 The Yatani mine area in central Honshu Island, Japan, was selected for this study.
51 The area includes a closed non-ferrous sulfide mine that had been producing galena,
52 sphalerite, native Au, and argentite. The objectives of the study were to evaluate the

53 geological and hydrological characteristics of the mine, to identify important minerals,
54 and to determine their roles in the formation of mine drainage (AMD and neutral mine
55 drainage). Groundwater flow systems in the mine area were evaluated through water
56 quality and isotopic studies interpreted by principal component analysis (PCA).
57
58 **2. Materials and methods**
59 *2.1 Geology and history of the Yatani mine*
60 The Yatani mine area is located 28 km southwest of Yonezawa City, within the
61 Bandai–Asahi National Park (Fig. 1). It is situated in the green tuff area of northeast
62 Japan, and includes a granitic basement overlain by Tertiary–Miocene volcanic and
63 sedimentary rocks. Surface mining began in 1870 after the discovery of Au ore
64 outcrops. When these were exhausted, mining continued underground for several
65 decades. Taihei Mining Co. Ltd acquired mining rights to the area in 1952 and began
66 mining Pb and Zn ores. By 1978 the monthly crude ore output was >10,000 tons with
67 average Pb and Zn grades of 2% and 4.4%, respectively. Decreasing metal prices and
68 the appreciating Japanese yen eventually made the operation unprofitable, and it closed
69 in 1988 (Sato et al., 1978).
70 The Yatani mineral deposit is of hydrothermal origin, formed within green tuff host
71 rock. It includes two types of veins: one rich in Pb and Zn, and the other containing Au
72 and Ag. The Pb–Zn ore deposits constitute the main veins of the mine, reaching a
73 maximum width of ~10 m and closely following NE–SW- and E–W-trending faults in
74 the area. The Pb–Zn veins comprise mainly quartz, galena, sphalerite, pyrite, calcite,
75 and chlorite and sometimes include native Au and argentite. The Au–Ag ore veins
76 contain quartz, native Au, argentite, pyrite, and rhodochrosite. In both types of veins,

77 ore minerals exhibit striped textures, indicating that quartz crystallized first, followed by
78 precipitation of galena and zincblende, and finally by deposition of native Au and
79 argentite (Taniguchi, 1969).
80 Two mining methods were employed at the mine, involving the cut-and-fill method
81 in deeper parts using sand, slime, and tailings as filling materials that did not
82 consolidate with cement; and the shrinkage-stoping method in shallower parts. A
83 mineral concentration system with its own power substation and repair facilities was
84 constructed underground. The adit mouth of the drainage level (level –2L) is located at
85 elevations of 626 and 2,280 m from the shaft. The tunnel extends from the bottom level
86 (–10 L) to the top (+2 L) level with a height difference of 600 m and runs E–W for ~2.5
87 km. Old mine workings deeper than the drainage level (level –2L) are kept submerged,
88 and AMD from the drainage level is presently treated by neutralization.
89
90 *2.2 Water sample collection and analysis*
91 Water samples were collected on 9 and 10 November 2008, from locations shown in
92 Figs 1 and 2. In the old mine workings (mining levels, drifts, and a shaft), samples were
93 collected from the shaft and other prominent parts of mine workings where significant
94 discharge of groundwater was observed, for example, from cracks in drainage level
95 walls, and fallen water from the back of the drift and the top of the shaft. Samples were
96 also collected from several points in major rivers and streams traversing the mining
97 area. All samples were stored in 1 L polypropylene bottles before filtering through 0.22
98 μm membrane filters. Temperature, pH, electrical conductivity (EC), and oxidation–
99 reduction potential (ORP) were measured on-site using a thermo-pH meter (KS-701,
100 Shindengen Electric Manufacturing Co. Ltd., Japan), an EC meter (B-173, Horiba Ltd.,

Japan), and an ORP meter (RM-12P, DKK-TOA Co., Japan), respectively. The ORP meter was equipped with an Ag–AgCl electrode, and measured values were converted to standard redox potentials (Eh) by adding a temperature-dependent constant for the electrode solution. The AMD flux on 9 November 2008, when mine drainage samples were taken, was 2.58 $m^3\ min^{-1}$. There was no rainfall on 10 November 2008 when river water was sampled; precipitation during the 30 days before sampling total 110 mm (Fig. 3).

All sample analyses were performed at the Analytical Center of Mitsubishi Materials Techno Corporation. Major anions (Cl^- and SO_4^{2-}) were analyzed by ion chromatography using Dionex DX-120 and IonPac As14 resin columns (Nippon Dionex K.K., Japan). Major cations (Na^+, K^+, Ca^{2+}, and Mg^{2+}), total Fe, and total Mn were analyzed by either inductively coupled plasma mass spectrometry (ICP–MS; Agilent 7700X, Agilent Technologies Japan Ltd., Japan) or inductively coupled plasma atomic emission spectroscopy (ICP–AES; ICAP-575, Thermo Fisher Scientific K.K., Japan). Alkalinity was determined by titration with 0.01 M H_2SO_4 to pH 4.8. Charge balances were within ±5%, indicating that all major cations and anions were adequately quantified. Analytical uncertainties of ICP–MS, ICP–AES, and ion chromatography results were all 2%–5%.

Oxygen isotopic ratios were determined by the CO_2 equilibration method (Epstein and Mayeda, 1953) and hydrogen isotopic ratios by the method of Coleman et al. (1982). $\delta^{18}O$ ($1000((^{18}O/^{16}O)_{sample}/(^{18}O/^{16}O)_{VSMOW}) - 1$), ‰) and δD ($1000((^{2}H/^{1}H)_{sample}/(^{2}H/^{1}H)_{VSMOW}) - 1$), ‰) values were calculated relative to Vienna Standard Mean Ocean Water (VSMOW) with analytical precisions of 0.1‰ and 1‰, respectively.

125

126 *2.3 Principal component analysis*

127 Principal component analysis (PCA) is a multivariate statistical technique used to
128 reduce complex high-dimensional data sets by converting observations into sets of
129 values or "principal components" (PC) related to original system components (Abdi and
130 Williams, 2010). The approach is ideal for geochemical surveys because each sample is
131 described by multiple factors such as pH, Eh, EC, and ion concentrations. PCA has been
132 applied in many studies comparing the qualities of groundwater, spring water, and river
133 water, and also in the classification of hot-spring waters (Masumoto and Hibiya, 1996;
134 Takamatsu, 1986; Mahlknecht et al., 2003).

135 Here, PCA was performed using the multivariate analysis software Pirouette LE ver.
136 3.11 (GL Sciences Inc., Japan), and it was applied to four variables measured on site
137 (temperature, pH, EC, and Eh), the concentrations of seven major ions (Na^+, K^+, Ca^{2+},
138 Mg^{2+}, Cl^-, HCO_3^-, and SO_4^{2-}), and the isotopic ratios δD and δ^{18}O. For normalization of
139 variables, logarithms were used for ion concentrations, and measured values for the four
140 factors measured on site, and isotopic ratios were the antilogs of the measured values.

141

142 3. **Results and discussion**

143 *3.1 Geochemical properties of water samples*

144 The geochemical and isotopic properties of water samples collected from the Yatani
145 mine area are summarized in Table 1 and their corresponding water chemistry displayed
146 in Stiff (Figs 1 and 2) and Piper diagrams (Fig. 4).

147

148 *3.1.1 River water*

149 The pH, EC, Eh, and temperature of river water samples are in the ranges of 6.0–
150 8.9, 1.8–9.1 mS m^{-1}, +353 to +579 mV, and 4.6°C–7.9°C, respectively. Concentrations
151 of major ions vary with location, with Ca^{2+}, Na^{+}, and HCO_3^- being dominant
152 downstream in the Yatanizawa River and the Tengusawa River (Na^{+}–HCO_3^- or
153 Ca^{2+}–HCO_3^- type waters (samples R-1, R-2, R-9, R-10, R-11, R-12, R-13, and R-14),
154 while SO_4^{2-} predominates in samples (Ca^{2+}–SO_4^{2-} type water; samples R-3, R-4, R-5,
155 R-6, R-7, and R-8) collected upstream where mineralized zones and veins are located
156 (Sato et al., 1978).
157
158 *3.1.2 Mine drainage*
159 The pH, EC, Eh, and temperature of mine drainage are in the ranges of 2.9–7.8,
160 16.5–381 mS m^{-1}, +304 to +656 mV, and 11.6°C–18.7°C, respectively. Mine drainage
161 samples are Ca^{2+}–SO_4^{2-} type waters, except for sample M-1 (from near the adit mouth),
162 which is a Ca^{2+}–HCO_3^- type water. Mine drainage samples M-1 to M-14 from old mine
163 workings has lower pH and higher EC values than river water, indicating significant
164 impact of AMD on groundwater quality. EC, pH, and major ion concentrations of mine
165 drainage also varies with location, with EC values increasing with decreasing pH from
166 adit mouth to veins and shaft (Fig. 5). Drainage sample M-12, from the drift, has the
167 highest EC (381 mS m^{-1}) and lowest pH (2.9). Sample M-11, from the shaft, has high
168 EC (235 mS m^{-1}) and a pH of 3.1. A similar trend was observed with concentrations of
169 total Fe and Mn in mine drainage samples. Total Fe and Mn concentrations in samples
170 collected near the adit mouth (samples M-1 to M-9) were <2.5 and 4.2 mg L^{-1},
171 respectively, while those in samples from around veins, drift, and the shaft (samples M-
172 10 to M-14) were ~80 and ~50 times higher, respectively.

173

174 *3.2 Hydrogen and oxygen isotopic ratios*

175 The δD and δ^{18}O values of water samples are in the ranges of −67.1‰ to −55.6‰
176 and −10.8‰ to −8.7‰, respectively, with relationships illustrated in Fig. 6. Isotopic
177 data plot close to the meteoric water line (Craig, 1961; Dansgaard, 1964), and are very
178 similar to those of river water and rainwater collected in Yamagata Prefecture (Mizota
179 and Kusakabe, 1994). The Tengusawa River water samples from higher elevations
180 (~930 m; samples R-9 and R-10) have lower δ^{18}O and δD values, suggesting that the
181 relationship between elevation and isotopic ratios is likely due to isotopic fractionation
182 during precipitation (Dansgaard, 1964; Lawrence and White, 1991; Mizota and
183 Kusakabe 1994). The ranges of δ^{18}O and δD values in mine drainage approximate those
184 of river water, barring sample R-14. Rainwater in mine drainage is temporally
185 decoupled from that in river water, so isotopic ratios in river water may not display
186 significant seasonal variations, with ratios in mine drainage effectively being averaged
187 over influx and underground flow. The δ^{18}O and δD values of mine drainage also vary
188 with location (Fig. 7). Isotopic ratios of drainage from the drift and shaft (samples M-10
189 to M-4) are lower than those of samples from the drainage level (samples M-1 to M-9).
190 δ^{18}O and δD values of mine drainage from the drift and shaft are similar to those of
191 river water from higher elevations (samples R-9 and R-10; Fig. 6). Drainage from the
192 mine drainage level may thus originate in the Yatanizawa River and its tributaries,
193 whereas that from the drift and shaft may originate in river water at higher elevations
194 (>900 m).

195

196 *3.3 Principal component analysis*

PCA results are shown in Table 2. Three principal components (PC1, PC2, and PC3) were selected, which together account for more than 82% of the total variability in the dataset. This indicates that the water quality is dominated by these three factors. The first principal component (PC1) has high loadings for Ca^{2+}, Mg^{2+}, and SO_4^{2-} with values of >0.35, suggesting that the increase in ion concentrations in mine drainage may be attributed to water–mineral interactions within old mine workings. The high SO_4^{2-} loading in PC1 could be explained by the oxidation of pyrite (FeS_2), a common sulfide mineral in metal deposits and altered rocks. Pyrite oxidation is facilitated by Fe^{3+} formed through the oxidation of Fe^{2+} by dissolved oxygen (Singer and Stumm, 1970; Moses et al., 1987; Tabelin et al., 2017a, b). The high Ca^{2+} loading relates to reactions of calcite ($CaCO_3$) associated with Au–Ag veins and Pb–Zn veins (Taniguchi, 1969), and possibly to interactions of AMD with concrete used in the construction of the underground concentrator and its supporting facilities. The significant Mg^{2+} loading relates to reactions of AMD with the mineral chlorite $(Mg, Fe, Al)_6(Al, Si)_4O_{10}(OH)_8$ associated with Pb–Zn veins (Taniguchi, 1969) or with cementitious materials containing significant amounts of Mg^{2+}.

For the second principal component (PC2), there are high loadings for pH and HCO_3^-, with values of 0.40 and 0.52, respectively, as expected because of the well-established inverse relationship between pH and HCO_3^- concentration (Eang et al., 2018a, b).

The third principal component (PC3) has high loadings for H and O isotopic ratios (>0.60), possibly reflecting the strong correlation between them in water samples and the effect of isotopic fractionation during precipitation (Figs 6 and 7).

220 The sum of the contributions of PC1, PC2, and PC3 is 82% (Table 2), indicating
221 that the geochemistry of surface water and mine drainage are satisfactorily explained by
222 the three PCs.
223 Scatter plots of PC1 vs. PC2 and PC1 vs. PC3 are shown in Fig. 8a and b,
224 respectively. Two different groups of data are clearly observed in both plots, belonging
225 to the water samples collected from the river and old mine workings, respectively. The
226 river water samples are on the negative side of PC1 whereas the mine drainage samples
227 have positive PC1 loading values. This indicates the possibility of interactions between
228 groundwater and sulfide minerals, sand slime, and tailings back-filled into excavated
229 mine areas.
230 The PC2 coefficients of mine drainage samples range from positive to negative
231 values in the following order: M-13 > M-14 > M-12 > M-11. This shows that the source
232 of mine drainage in drifts (M-11 and M-12) did not come mainly from the shaft (M-13
233 and M-14). It is possible that a large portion of the water from M-11 and M-12
234 originated from the deeper reductive groundwater. This is consistent with the observed
235 flow pattern in which M-11 and M-12 represent water flowing from the back of the
236 drifts, M-13 was the water dripping from the top of the shaft, and M-14 was spring
237 water from the shaft.
238 According to the principal component scores of PC1 vs PC3 (Fig. 8b), two groups
239 of samples can be classified. The group of higher PC1 scores belongs to river water
240 from the elevation of <900 m and mine drainage from the drainage level. On the other
241 hand, the other group represents river water from the elevation of >900 m and mine
242 drainage samples from the drifts and the shaft. These results indicate that the main
243 source of mine drainage from the drainage level is from the Yatanizawa River while

mine drainage from the drifts and shaft were derived from surface water with higher elevation than that of the Yatanizawa River. In addition, the board distribution of PC1 with narrow PC3 scores on shift samples indicates the progress of water–mineral interactions from the same source of water, along the flow from the top to bottom in the shift, as represented by an arrow in Fig. 8b.

3.4 Concept of groundwater flow and discharge

A conceptual model of drainage flow was devised on the basis of results described in sections 3.1–3.3, as shown in Fig. 9. Groundwater infiltrating from the Yatanizawa River and its tributaries above the mine drainage level, and from the mountain slope (elevation > 900 m) north of the mining area, reacts with sulfide minerals, sand slime and tailings back-filled into excavated mine areas releasing SO_4^{2-}, Ca^{2+}, and Mg^{2+} before flowing out of the drainage level. In the PCA study, PC1 is related to the degree of water–rock interaction, PC2 to the contribution of groundwater from the deep reductive environment, and PC3 to correlation between H and O isotopic ratios and isotopic fractionation during precipitation. The total AMD flux measured at the neutralization treatment plant increased during the snowmelt season of March to May, with the pH decreasing over that time (Fig. 3). This suggests that the groundwater flux, infiltrating from the mountain slope to the excavated area and reacting with sulfide minerals, increased during the snowmelt season. It follows that a possible method of reducing AMD formation would be to prevent contact between dissolved oxygen and sulfide minerals by changing the drainage level from the current −2 level to the 0 level, or by filling the shallow underground excavated area with cementitious materials.

4. Conclusions

The findings of this geological, hydrological, geochemical, and isotopic study of acid mine drainage at the Yatani mine are as follows.

(1) AMD is formed through interactions between groundwater and sulfide minerals, sand slime, and tailings back-filled into excavated mine areas.

(2) The groundwater recharge area for AMD formation is located on the mountain slope at altitudes of ~900 m.

(3) AMD formation in the drifts and shaft is more pronounced than in the mine drainage level.

(4) Based on a conceptual model of groundwater flow at the mine, AMD formation could be reduced by preventing contact between dissolved oxygen and sulfide minerals by increase the drainage level, or by filling shallow underground excavated areas with cementitious materials.

Acknowledgments

The authors thank the editor and anonymous reviewers for their constructive comments that improved this manuscript. We also thank the staff of Mitsubishi Materials Corporation, Eco-Management Corporation, and Mitsubishi Materials Techno Corporation for their help, advice, and cooperation during this study.

References

Abdi, H., Williams, L. J., 2010. Principal component analysis. Wiley Interdisciplinary Reviews: Computational Statistics 2, 4, 433–459.

291 Boularbah, A., Schwartz, C., Bitton, G., Morel. J. L., 2006. Heavy metal contamination
292 from mining sites in South Morocco: I. Use of a biotest to assess metal toxicity of
293 tailings and soils. Chemosphere 63, 802–810.
294 Casiot, C., Lebrun, S., Morin, G., Bruneel, O., Personné, J. C., Elbaz-Poulichet, F.,
295 2005. Sorption and redox processes controlling arsenic fate and transport in a stream
296 impacted by acid mine drainage. Sci. Total Environ. 347, 122–130.
297 Coleman, M. L., Shepherd, T. J., Durham, J. J., Rouse, J. E., Moore, G. R., 1982.
298 Reduction of water with zinc for hydrogen isotope analysis. Anal. Chem. 54, 993–
299 995.
300 Craig, H., 1961. Standard for reporting concentrations of deuterium and oxygen-18 in
301 natural waters. Science 133, 1833–1834.
302 Dansgaard, W., 1964. Stable isotopes in precipitation. Tellus 16, 436–438.
303 Eang, K. E., Igarashi, T., Fujinaga, R., Kondo, M., Tabelin, C. B., 2018a. Groundwater
304 monitoring of an open-pit limestone quarry: Groundwater characteristics, evolution
305 and their connections to rock slopes. Environ. Monit. Assess. 190, 193.
306 Eang, K. E., Igarashi, T., Kondo, M., Nakatani, T., Tabelin C. B., Fujinaga, R., 2018b.
307 Groundwater monitoring of an open-pit limestone quarry: Water–rock interaction
308 and mixing estimation within the rock layers by geochemical and statistical
309 analyses. Int. J. Min. Sci. Technol. 28, 849–857.
310 Epstein, S., Mayeda, T., 1953. Variation of the ^{18}O content of waters from natural waters.
311 Geochim. Cosmochim. Acta 4, 213–224.
312 Gammons, C. H., Duaime, T. E., Parker, S. R., Poulson, S. R., Kennelly, P., 2010.
313 Geochemistry and stable isotope investigation of acid mine drainage associated with
314 abandoned coal mines in central Montana, USA. Chemical Geology 269, 100–112.

315 Gault, A. G., Cooke, D. R., Townsend, A. T., Charnock, J. M., Polya, D. A., 2005.
316 Mechanisms of arsenic attenuation in acid mine drainage from Mount Bischoff,
317 western Tasmania. Sci. Total Environ. 345, 219–228.
318 Hazen, J. M., Milliams, M. W., Stover, B., Wireman, M., 2002. Characterization of acid
319 mine drainage using a combination of hydrometric, chemical and isotopic analyses,
320 Mary Murphy Mine, Colorado. Environ. Geochem. Health 24, 1–22.
321 Herrera, P., Uchiyama, H., Igarashi, T., Asakura, K., Ochi, Y., Ishizuka, F., Kawada, S.,
322 2007a. Acid mine drainage treatment through a two-step neutralization ferrite-
323 formation process in northern Japan: Physical and chemical characterization of the
324 sludge. Miner. Eng. 20, 1309–1314.
325 Herrera, P., Uchiyama, H., Igarashi, T., Asakura, K., Ochi, Y., Iyatomi, N., Nagae, S.,
326 2007b. Treatment of acid mine drainage through a ferrite formation process in
327 central Hokkaido, Japan: Evaluation of dissolved silica and aluminium interference
328 in ferrite formation. Miner. Eng. 20, 1255–1260.
329 Hien, N. T. T., Yoneda, M., Matsui, A., Hai, H. T., Pho, N. V., Quang, N. H., 2012.
330 Environmental contamination of arsenic and heavy metals around Cho Dien lead
331 and zinc mine, Vietnam. J. Water Environ. Technol. 10, 253–265.
332 Hierro, A., Olías, M., Cánovas, C. R., Martín, J. E., Bolivar, J. P., 2014. Trace metal
333 partitioning over a tidal cycle in an estuary affected by acid mine drainage (Tinto
334 estuary, SW Spain). Sci. Total Environ. 18–28, 497–498.
335 Iwatsuki, T., Yoshida, H., 1999. Groundwater chemistry and fracture mineralogy in the
336 basement granitic rock in the Tono uranium mine area, Gifu Prefecture, Japan:
337 Groundwater composition Eh evolution analysis by fracture filling minerals.
338 Geochem. J. 33, 19–32.

339 Kalin, M., Fyson, A., Wheeler, W. N., 2006. The chemistry of conventional and
340 alternative treatment systems for the neutralization of acid mine drainage. Sci. Total
341 Environ. 366, 395–408.
342 Kawabe, N., 2017. The significance of the soil environment, aqueous environment and
343 planting trees measure in mine pollution control. Program and Abstracts, MMIJ and
344 EARTH 2017 Sapporo, pp. 89–90 (in Japanese).
345 Lawrence, J. R., White, S. D., 1991. In: Taylor, Jr., H. P., O'Neil, J. R., Kaplan, I. R., et
346 al. (Eds.), A Tribute to Samuel Epstein. The Geochemical Society. Special
347 Publication, No. 3, New York, pp. 169–185.
348 Lim, H. S., Lee, J. S., Chon, H. T., Sager, M., 2008. Heavy metal contamination and
349 health risk assessment in the vicinity of the abandoned Songcheon Au–Ag mine in
350 Korea. J. Geochem. Explor. 96, 223–230.
351 Lowson, R.T., 1982. Aqueous oxidation of pyrite by molecular oxygen. Chem. Rev. 82,
352 461–497.
353 Mahara, Y., Nakata, E., Oyama, T., Miyakawa, K., Igarashi, T., Ichihara, Y.,
354 Matsumoto, K., 2006. Proposal for the methods to characterize fossil seawater:
355 Distribution of anions, cations and stable isotopes, and estimation on the
356 groundwater residence time by measuring ^{36}Cl at the Taiheiyou Coal Mine. J.
357 Groundwater Hyd. 48, 17–33 (in Japanese with English abstract).
358 Mahlknecht, J., Steinich, B., Navarro de Léon, I., 2003. Groundwater chemistry and
359 mass transfers in the independence aquifer, central Mexico, by using multivariate
360 statistics and mass-balance models. Environ. Geol. 45, 781-795.

361 Masumoto, K., Hibiya, K., 1996. Evaluation of regional groundwater flow in rock mass
362 by geochemical survey: A case study at tunneling site. J. Japan Soc. Eng. Geol. 36,
363 70–78 (in Japanese with English abstract).
364 Mizota, C., Kusakabe, M., 1994. Spatial distribution of δD–δ^{18}O values of surface and
365 shallow groundwaters from Japan, south Korea and east China. Geochem. J. 28,
366 387–410.
367 Molson, J. W., Fala, O., Aubertin, M., Bussière, B., 2005. Numerical simulations of
368 pyrite oxidation and acid mine drainage in unsaturated waste rock piles. J. Contam.
369 Hydrol. 78, 343–371.
370 Moses, C. O., Nordstrom, D. K., Herman, J. S., Mills, A. L., 1987. Aqueous pyrite
371 oxidation by dissolved oxygen and ferric iron. Geochim. Cosmochim. Acta 51,
372 1561–1571.
373 Nagai, Y., 2018. Action for the mountains of origin recurrence of closed mines which
374 utilized Green Remediation. Program and Abstracts, MMIJ Tokyo, pp. 36 (in
375 Japanese).
376 Ogino T., 2017. Water purification by constructed wetland. Program and Abstracts,
377 MMIJ and EARTH 2017 Sapporo, pp. 89 (in Japanese).
378 Okimoto, N., Yamagata, S., Mizukoshi, H., Sugimoto, H., Sakakibara, N., 2017.
379 Application of a soil erosion prevention method in the abandoned mine site by a
380 greening technology with cement and wood chips, “Chipcrete”. Program and
381 Abstracts, MMIJ and EARTH 2017 Sapporo, pp. 91–92 (in Japanese).
382 Okumura, M., 2003. Hydrogeochemical study of the 3M level adit drainage at the old
383 Matsuo mine. Resources Geol. 53, 173–182 (in Japanese with English abstract).

384 Pabst, T., Bussière, B., Aubertina, M., Molson, J., 2018. Comparative performance of
385 cover systems to prevent acid mine drainage from pre-oxidized tailings: A
386 numerical hydro-geochemical assessment. J. Contam. Hydrol. 214, 39–53.
387 Ramasamy, M., Power, C., Mkandawire, M., 2018. Numerical prediction of the long-
388 term evolution of acid mine drainage at a waste rock pile site remediated with an
389 HDPE-lined cover system. J. Contam. Hydrol. 216, 10–26.
390 Sato, N., Takatori, I., Yanagisawa, S., 1978. Geology and ore deposits of the Yatani
391 Mine, Yamagata Prefecture, Japan, with special reference to some suggestions on
392 exploration. Mining Geol. 28, 177–190 (in Japanese with English abstract).
393 Singer, P. C., Stumm, W., 1970. Acidic mine drainage: The rate-determining step.
394 Science 167, 1121–1123.
395 Skierszkan, E. K., Mayer, K. U., Weis, D., Beckie, R. D., 2016. Molybdenum and zinc
396 stable isotope variation in mining waste rock drainage and waste rock at the
397 Antamina mine, Peru. Sci. Total Environ. 550, 103–113.
398 Sracek, O., Choquette, M., Gélinas, P., Lefebvre, R., Nicholson, R. V., 2004.
399 Geochemical characterization of acid mine drainage from a waste rock pile, Mine
400 Doyon, Quebec, Canada. J. Contam. Hydrol. 69, 45–71.
401 Tabelin, C. B., Igarashi, T., Takahashi, R., 2012a. Mobilization and speciation of
402 arsenic from hydrothermally altered rock in laboratory column experiments under
403 ambient conditions. Appl. Geochem. 27, 326–342.
404 Tabelin, C. B., Igarashi, T., Yoneda, T., 2012b. Mobilization and speciation of arsenic
405 from hydrothermally altered rock containing calcite and pyrite under anoxic
406 conditions. Appl. Geochem. 27, 2300–2314.

Tabelin, C. B., Sasaki, R., Igarashi, T., Park, I., Tamoto, S., Arima, T., Ito, M., Hiroyoshi, N., 2017a. Simultaneous leaching of arsenite, arsenate, selenite and selenate, and their migration in tunnel-excavated sedimentary rocks: I. Column experiments under intermittent and unsaturated flow. Chemosphere 186, 558–569.

Tabelin, C. B., Veerawattananun, S., Ito, M., Hiroyoshi, N., Igarashi, T., 2017b. Pyrite oxidation in the presence of hematite and alumina: I. Batch leaching experiments and kinetic modeling calculations. Sci. Total Environ. 580, 687–698.

Tabelin, C. B., Veerawattananun, S., Ito, M., Hiroyoshi, N., Igarashi, T., 2017c. Pyrite oxidation in the presence of hematite and alumina: II. Effects on the cathodic and anodic half-cell reactions. Sci. Total Environ. 581–582, 126–135.

Tabelin, C. B., Sasaki, R., Igarashi, T., Park, I., Tamoto, S., Arima, T., Ito, M., Hiroyoshi, N., 2017d. Simultaneous leaching of arsenite, arsenate, selenite and selenate, and their migration in tunnel-excavated sedimentary rocks: II. Kinetic and reactive transport modeling. Chemosphere 188, 444–454.

Takamatsu, N., 1986. Classification of coastal type saline springs by principal component analysis. J. Hot Spring Science 36, 158–166 (in Japanese with English abstract).

Taniguchi, H., 1969. Geology and ore deposits of the Yatani Mine, with special reference to the gold and silver veins. Mining Geol. 19, 113–121 (in Japanese with English abstract).

Tomiyama, S., Ueda, A., Ii, H., Nakamura, Y., Koizumi, Y., Saito, K., 2010a. Sources and flow system of groundwater in the Hosokura mine, Miyagi Prefecture, using geochemical method and numerical simulation. J. MMIJ 126, 31–37 (in Japanese with English abstract).

Tomiyama, S., Ii, H., Koizumi, Y., Metugi, H., 2010b. Modeling of groundwater recharge and discharge in Tomitaka mine, Miyazaki Prefecture. J. Groundwater Hyd., 52, 261–274 (in Japanese with English abstract).

Tomiyama, S., Takahashi, K., Yamagata, S., Igarashi, T., 2016a. Study the effect of sealing ground surface on reduction of mine drainage. Program and Abstracts, MMIJ Morioka, pp. 130 (in Japanese).

Tomiyama, S., Igarashi, T., Ii, H., Takano, H., 2016b. Sources and flow system of groundwater in the Shimokawa mine, north Hokkaido, using geochemical method and numerical simulation. J. MMIJ 132, 80–88 (in Japanese with English abstract).

Ueda, H., Masuda, N., 2005. An analysis of mine drainage treatment cost and the technical development to prevent mine pollution. J. MMIJ 121, 323–329 (in Japanese with English abstract).

Wunsch, D. R., Dinger, J. S., Graham, D. R., 1999. Predicting groundwater movement in large mine spoil areas in the Appalachian Plateau. Int. J. Coal Geol. 41, 73–106.

Yamaguchi, K., Tomiyama, S., Metugi, H., Ii, H., Ueda, A., 2015. Flow and geochemical modeling of drainage from Tomitaka mine, Miyazaki, Japan. J. Environ. Sci. 36, 130–143.

Younger, P. L., 2001. Mine water pollution in Scotland: Nature, extent and preventative strategies. Sci. Total Environ. 265, 309–326.

Zhao, Q., Guo, F., Zhang, Y., Ma, S., Jia, X., Meng, W., 2017. How sulfate-rich mine drainage affected aquatic ecosystem degradation in northeastern China, and potential ecological risk. Sci. Total Environ. 609, 1093–1102.

Table 1. Geochemical properties of water samples.

Sample type	Sample	pH	EC (mS m^{-1})	Eh (mV)	Temp (°C)	Concentration (mg L^{-1})									Stable isotope ratios (‰)	
						Na^+	K^+	Ca^{2+}	Mg^{2+}	Cl^-	HCO_3^-	SO_4^{2-}	T-Fe	T-Mn	δD	δ^{18}O
River water	R-1	8.9	2.6	353	7.9	2.2	0.3	2.5	0.5	1.9	7.8	4.3	<0.1	<0.1	–61.4	–10.1
	R-2	8.5	9.1	392	6.2	2.3	0.6	18	1.3	2.1	35	23	<0.1	<0.1	–61.7	–10.1
	R-3	8.1	3.7	412	5.0	1.6	0.7	4.4	0.7	1.8	4.4	11	<0.1	0.2	–64.2	–10.4
	R-4	6.0	4.0	525	7.1	1.8	1.9	3.6	0.7	2.1	0.7	15	<0.1	0.1	–60.9	–10.2
	R-5	6.4	4.9	472	6.5	2.7	1.0	6.8	0.6	1.7	9.2	16	<0.1	0.2	–60.6	–10.3
	R-6	6.9	6.2	414	4.6	3.2	0.6	9.9	0.9	1.9	14	21	0.1	<0.1	–61.8	–9.7
	R-7	6.7	3.5	579	5.6	2.7	0.8	4.4	0.4	1.6	7.4	11	<0.1	<0.1	–64.1	–10.3
	R-8	6.7	4.2	507	7.3	2.0	1.5	4.8	1.0	2.1	6.6	13	<0.1	<0.1	–67.1	–10.5
	R-9	6.7	2.1	498	5.5	2.5	0.5	2.1	0.3	1.6	11	1.7	<0.1	<0.1	–69.4	–10.8
	R-10	6.7	1.8	497	6.4	2.3	1.0	1.0	0.3	1.7	8.9	1.0	<0.1	<0.1	–67.7	–10.7
	R-11	6.7	2.0	514	6.8	2.4	0.5	1.7	0.4	1.9	8.6	1.8	0.5	0.1	–64.1	–10.1
	R-12	6.9	3.9	511	6.1	3.2	0.6	5.4	0.7	1.8	22	4.4	0.2	<0.1	–69.4	–10.6
	R-13	6.9	3.6	515	6.5	2.3	0.7	5.4	1.1	1.8	13	10	<0.1	<0.1	–65.9	–10.4
	R-14	7.1	5.2	517	6.2	2.6	0.8	7.6	1.5	2.1	18	11	<0.1	<0.1	–55.6	–8.7
	R-15	6.9	4.6	512	6.4	3.2	0.7	6.4	0.5	1.7	14	11	<0.1	<0.1	–65.2	–10.5
Mine drainage from drainage level (–2L)	M-1	7.6	16.5	512	11.6	5.5	0.7	29	1.8	2.4	70	32	<0.1	<0.1	–63.8	–10.2
	M-2	7.4	22.6	516	13.5	6.1	1.0	43	2.2	2.3	78	62	0.2	1.9	–63.9	–10.2
	M-3	7.4	29.2	518	12.6	5.5	1.3	59	2.4	2.2	93	88	0.1	0.4	–64.1	–10.4
	M-4	7.4	32.6	480	12.8	6.2	1.1	66	2.0	2.2	54	130	<0.1	0.3	–63.2	–10.0
	M-5	7.4	37.2	478	12.0	3.3	1.3	73	5.6	2.2	57	160	2.5	4.2	–64.6	–10.6
	M-6	7.8	70.7	477	16.6	6.8	1.0	66	1.6	2.1	53	130	<0.1	1.6	–65.0	–10.6
	M-7	7.6	73.6	439	17.4	18	1.3	120	3.6	2.3	110	260	<0.1	0.5	–66.1	–10.6
	M-8	7.1	97.2	304	17.1	17	1.7	210	8.9	2.3	260	380	<0.1	2.1	–63.7	–9.9
	M-9	7.0	37.5	455	17.2	10	2.0	230	8.4	2.1	220	400	<0.1	<0.1	–63.4	–10.4
	M-10	5.4	70.7	459	18.3	8.3	1.8	340	17	2.2	230	770	22	33	–61.1	–10.0
Mine drainage from drifts	M-11	2.9	381	476	17.8	5.4	4.3	290	85	2.1	0	3200	210	210	–67.1	–10.7
	M-12	3.1	235	452	17.7	6.3	3.3	170	45	2.2	0	1500	47	170	–64.9	–10.7
Mine drainege from shaft	M-13	6.7	32.8	432	16.8	15	0.4	39	1.0	2.0	61	80	1.4	0.3	–66.7	–10.8
	M-14	5.6	127	656	18.7	14	2.7	210	19	1.9	34	810	89	62	–66.1	–10.8

Table 2. Factor loadings and contributions of principal components (PCs).

Variables		PC1	PC2	PC3
pH		–0.26	0.40	–0.01
EC		0.33	-0.19	–0.12
Eh		0.12	-0.46	–0.03
Temperature		0.36	0.23	–0.10
Chemical composition	Na^+	0.29	0.33	–0.12
	K^+	0.31	–0.21	0.12
	Ca^{2+}	0.35	0.26	0.06
	Mg^{2+}	0.39	0.04	0.08
	Cl^-	0.24	0.12	0.34
	SO_4^{2-}	0.38	0.11	0.12
	HCO_3^-	–0.12	0.52	–0.02
Stable isotopes	δD	–0.06	–0.08	0.66
	$\delta^{18}O$	–0.11	0.09	0.60
Rate of contribution (%)		46.3	23.1	13.2

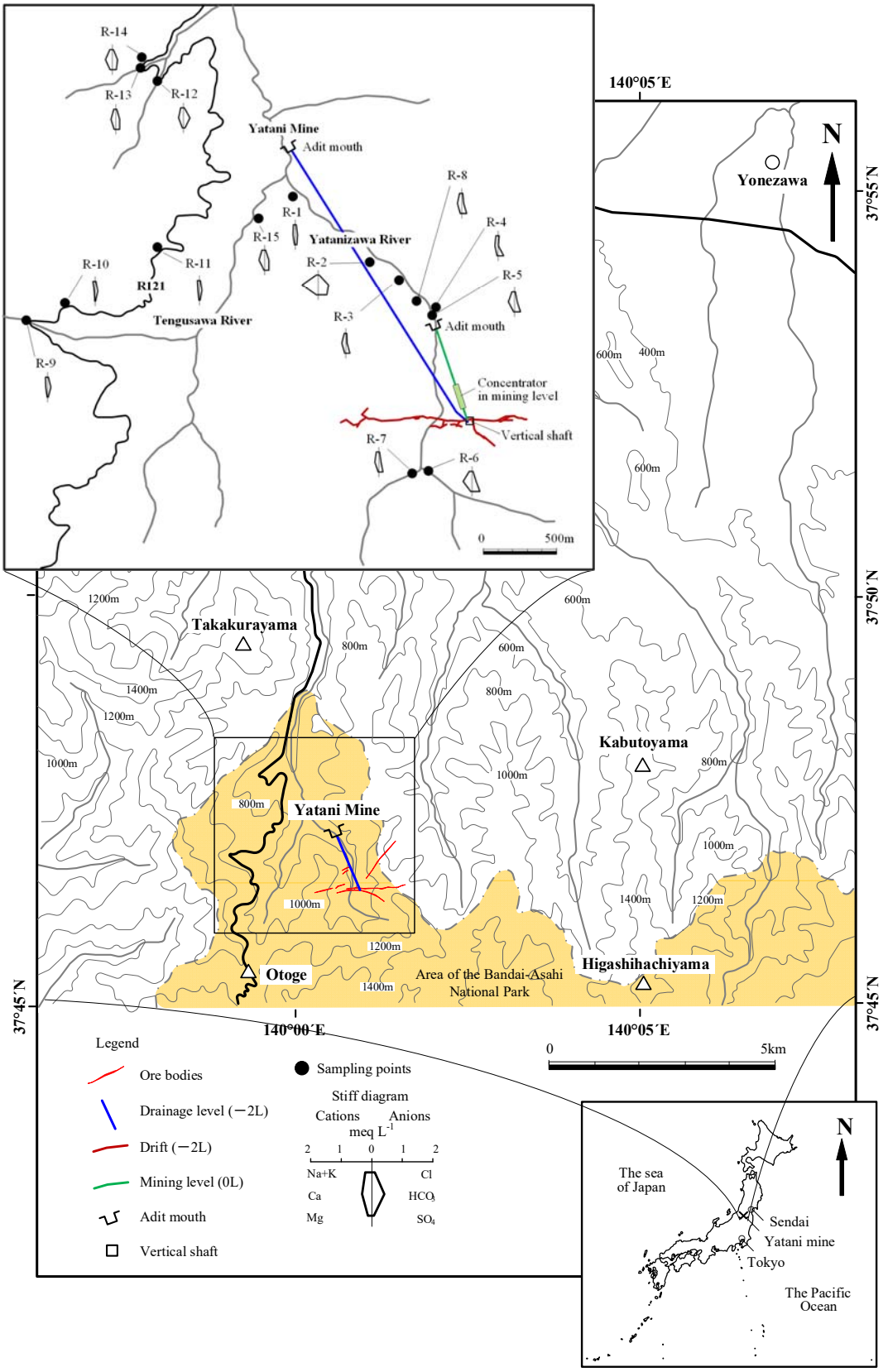

Fig. 1. Location of water sampling points, with corresponding water sample properties indicated by Stiff diagrams.

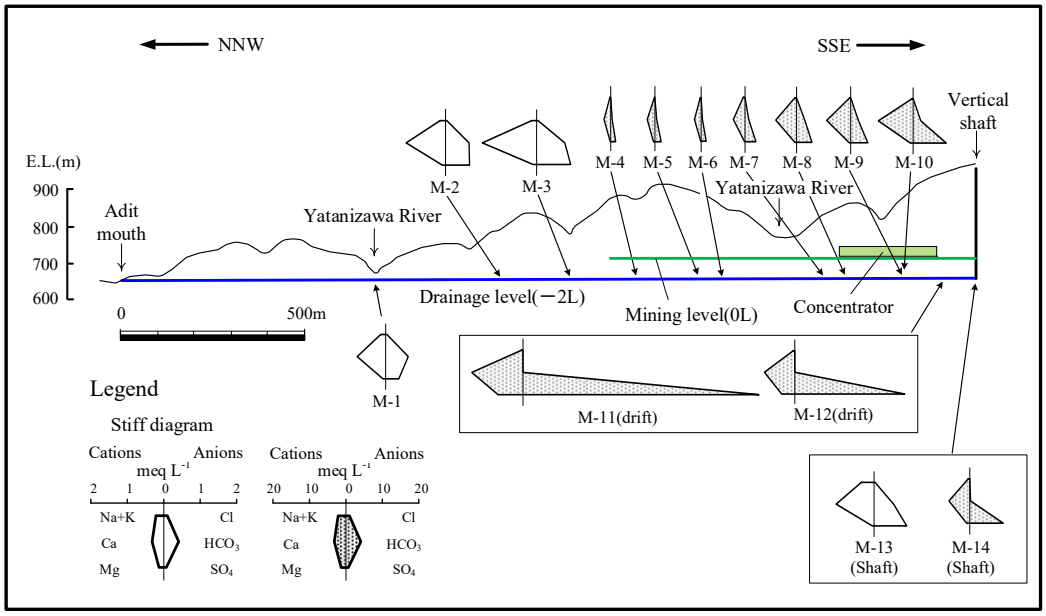

Fig. 2. Stiff diagrams of mine drainage samples from the drainage level (–2L), including samples collected from the drift and shaft (note that the concentrations in shaded Stiff diagrams are 10 times higher than those in unshaded diagrams).

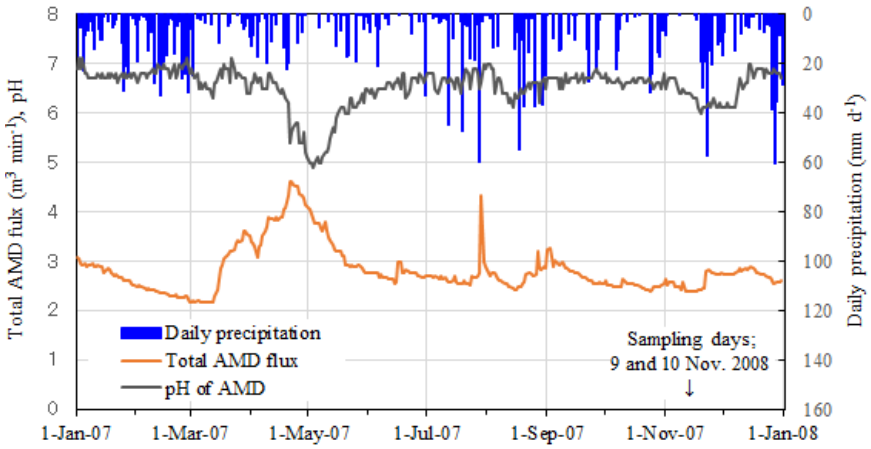

Fig. 3. Relationships between precipitation, total AMD flux, and pH measured at the neutralization treatment plant.

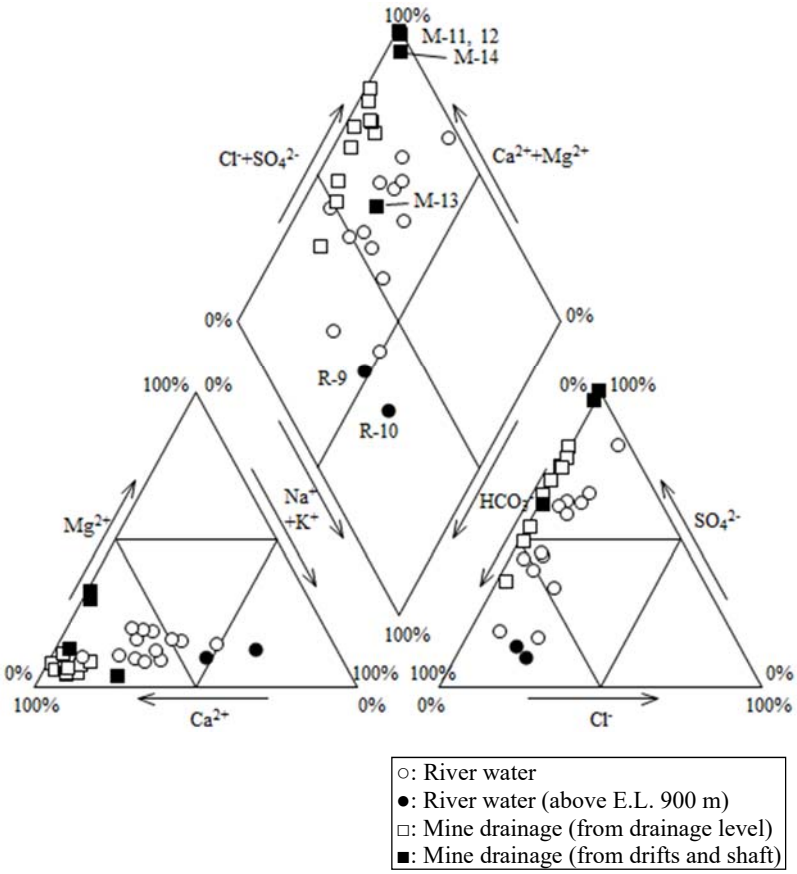

Fig. 4. Piper diagram showing the hydrochemical facies of river water, mine drainage, and AMD samples collected from the Yatani mine area.

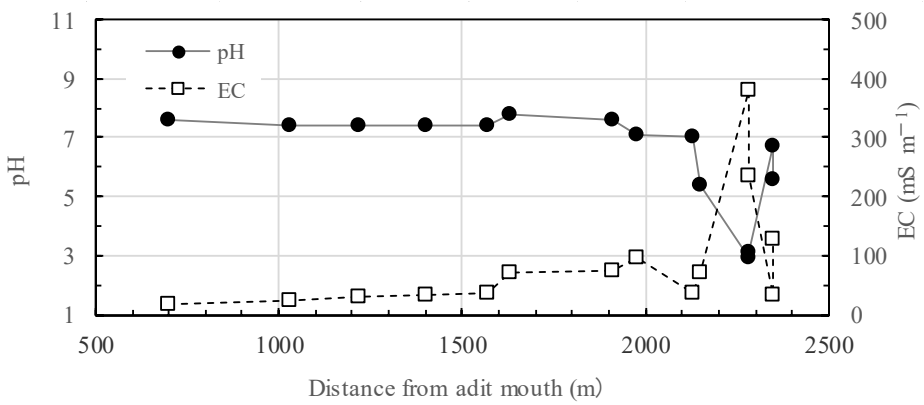

Fig. 5. Spatial variations in pH and EC of mine drainage samples along the mine drainage level.

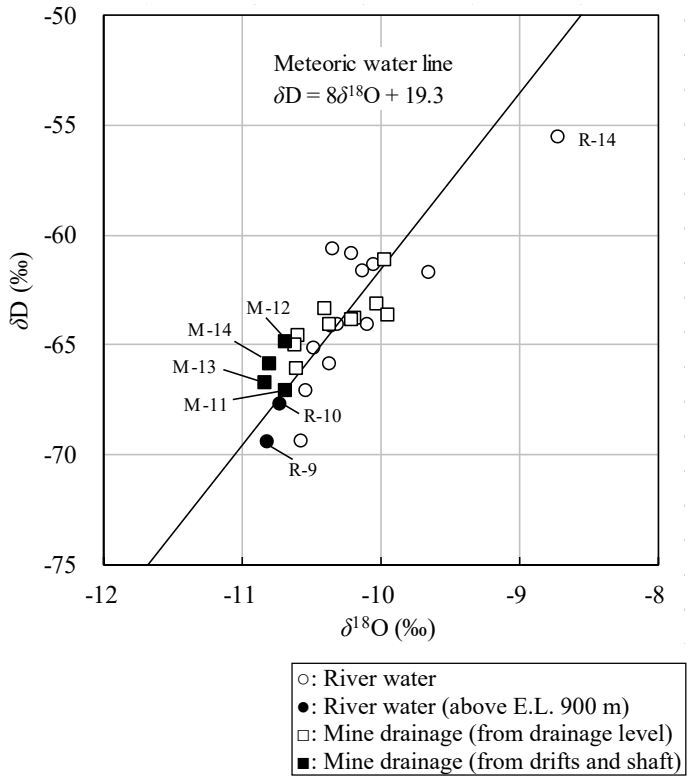

Fig. 6. Relationship between δD and δ^{18}O values of water samples, relative to the meteoric water line.

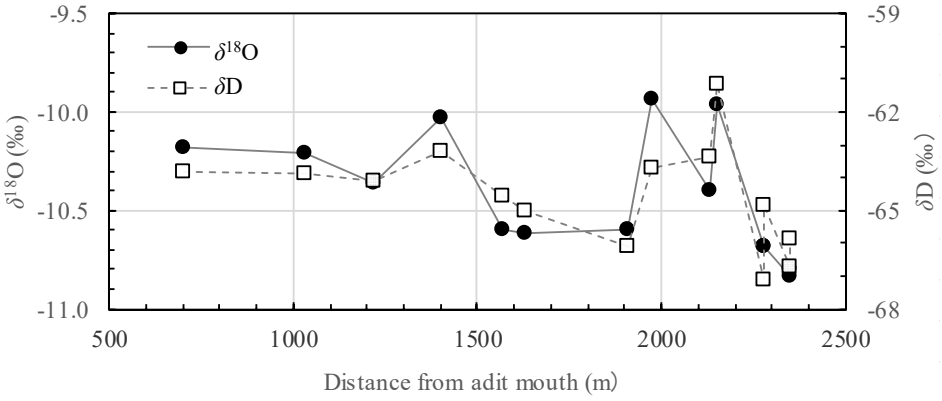

Fig. 7. Spatial distribution of δD and δ^{18}O values of mine drainage samples along the drainage level.

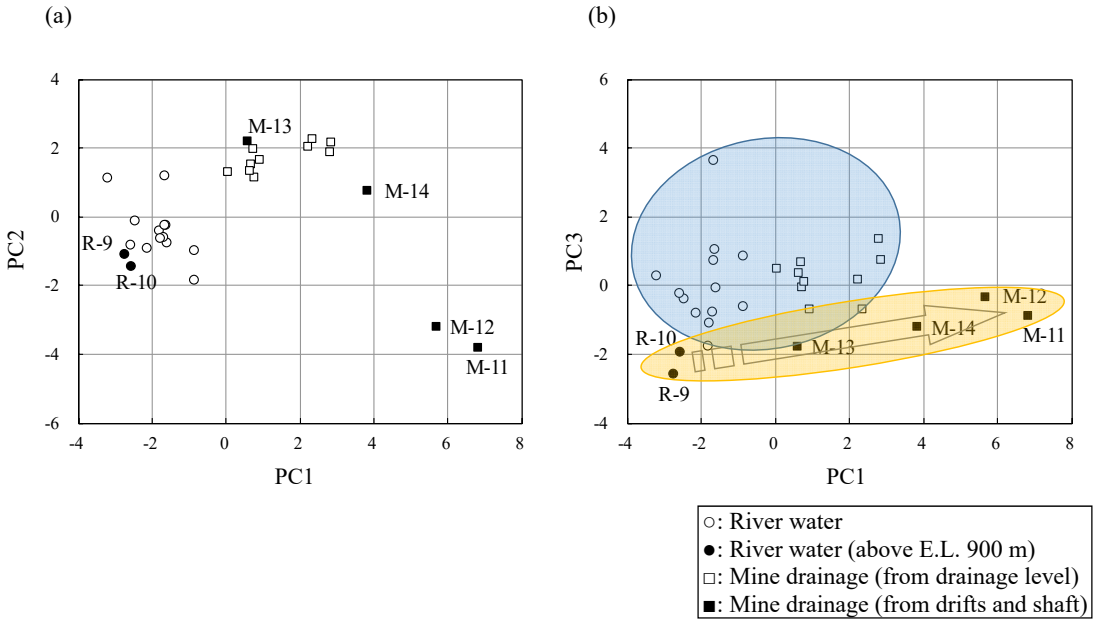

Fig. 8. PCA principal component scores of (a) PC2 vs. PC1 and (b) PC3 vs. PC1.

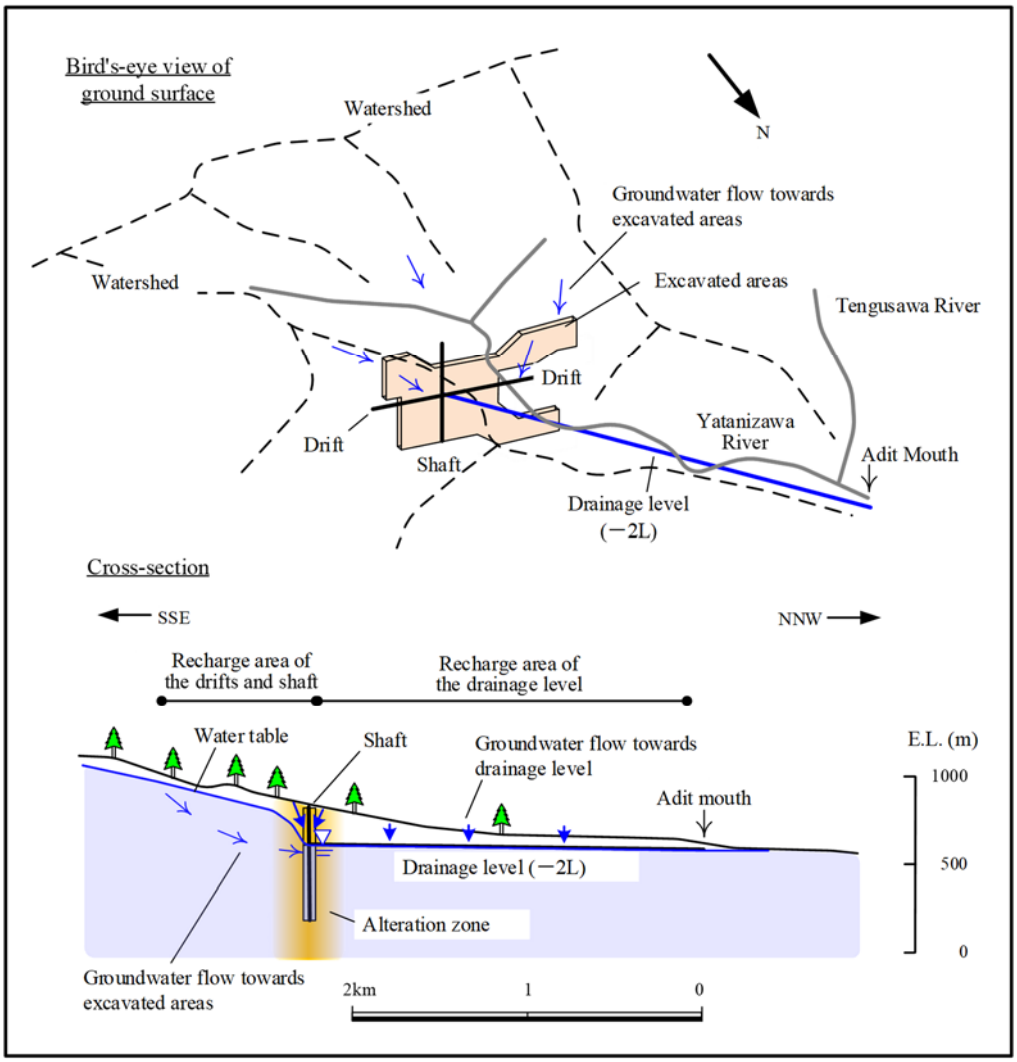

Fig. 9. Conceptual model of groundwater flow and discharge.